MATERIALS PHYSICS AND MECHANICS RESEARCH ARTICLE

Submitted: April 30, 2026 **Revised: May 18, 2026** **Accepted: June 12, 2026**

Determining the effective radius of a triple junction of grain boundaries using molecular dynamics

G.M. Poletaev [1]✉, Y.V. Bebikhov [2], A.S. Semenov [2], R.Y. Rakitin [3], D.V. Novoselova [4]

[1] Polzunov Altai State Technical University, Barnaul, Russia

[2] Polytechnic Institute of North-Eastern Federal University, Mirny, Russia

[3] Altai State University, Barnaul, Russia

[4] Kuzbass Institute of the Federal Penitentiary Service of Russia, Novokuznetsk, Russia

✉ gmpoletaev@mail.ru

ABSTRACT

Two methods are proposed for determining the effective radius of triple junctions of grain boundaries based on the analysis of the self-diffusion coefficient distribution in the junction region and the potential energy distribution of atoms. Both methods are considered using the example of triple junctions of high-angle tilt boundaries with <100> and <111> misorientation axes in nickel with varying contents of excess free volume. Triple junctions in the model were created by simulating the crystallization of a melt from three differently oriented crystalline seeds. Excess free volume was introduced into the triple junction by removing the corresponding number of atoms from the initial computational cell. During crystallization, the introduced free volume concentrated predominantly in the grain boundaries and triple junction regions, with the free volume fraction increasing toward the junction site. With increasing excess free volume in the triple junctions, self-diffusion proceeded more intensively. The diffusion intensity within the triple junction itself was generally distributed non-uniformly and increased toward the junction center. It is shown that the effective radius of the triple junction, determined using both methods based on the diffusion coefficient and atomic energy distributions, increases with the free volume content.

KEYWORDS

molecular dynamics • triple junction • grain boundary • tilt boundary • diffusion

Citation: Poletaev GM, Bebikhov YV, Semenov AS, Rakitin RY, Novoselova DV. Determining the effective radius of a triple junction of grain boundaries using molecular dynamics. *Materials Physics and Mechanics*. 2026;54(4): 53–64.
http://dx.doi.org/10.18149/MPM.5442026_6

Introduction

A triple junction (TJ) of grain boundaries is a linear defect along which three grain boundaries meet. TJs, along with grain boundaries, play an important role in various properties of polycrystals, particularly those related to deformation and diffusion [1–9]. According to experimental data, diffusion along most TJs proceeds significantly more intensively than along the grain boundaries that form them [1,2,10,11]. In addition, TJs play a crucial role in processes associated with plastic deformation, dislocation generation and blocking, and recrystallization [2,3,8]. The contribution of TJs to the properties of polycrystals increases with decreasing grain size and becomes significant in the case of ultrafine-grained and especially nanocrystalline materials [2–4].

Triple junctions are often characterized by a looser structure with a higher free volume content compared to the grain boundaries that form them. Some researchers even

© G.M. Poletaev, Y.V. Bebikhov, A.S. Semenov, R.Y. Rakitin, D.V. Novoselova, 2026.
Publisher: Peter the Great St. Petersburg Polytechnic University
This is an open access article under the CC BY-NC 4.0 license (https://creativecommons.org/li-censes/by-nc/4.0/)

note the presence of amorphous phase inclusions in TJs . In this regard, a number of studies report the “premelting” phenomenon of triple junctions [12–14], which consists in the fact that melting of polycrystals begins predominantly at triple junctions and other similar defects with relatively high free volume content.

Meanwhile, in some studies, for example in [15,16], when attempting to simulate the structure of TJs and diffusion along them using the molecular dynamics method, it was found that diffusion along them was almost indistinguishable from diffusion along grain boundaries. This contradiction with experimental data can, on one hand, be explained by the existence of different types of TJs in polycrystals, differing in structure and properties. Thus, according to the work [17], TJs should be classified into at least two types: stress-free (or equilibrium) ones, which do not contain excess defects, and stressed (non-equilibrium) ones, which contain excess dislocations and disclinations, second-phase particles, and other defects. In real experiments, the existence of "structurally perfect" equilibrium TJs has indeed been confirmed, however, the question of their relatively low fraction in polycrystals remained unresolved – non-equilibrium junctions containing excess free volume are generally present in significantly greater numbers than equilibrium ones [1,2].

In [18], using molecular dynamics modeling, we analyzed various reasons for the formation of excess free volume in TJs. We concluded that excess free volume forms in junctions primarily during the crystallization stage due to the locking (fixation) of the liquid phase density upon the meeting of three crystallization fronts, which transform into grain boundaries, while the triple junction region crystallizes last. As a result, excess free volume concentrates in the TJ after solidification. A second reason may be the accumulation of dislocations (or Burgers vector accumulation) during grain boundary sliding under deformation, leading to the formation of a dislocation or disclination complex in the junction. However, we consider this a secondary possible cause.

For analyzing TJ properties, an important characteristic is its effective radius. It is clear that this linear defect does not have a sharp boundary, and estimating its radius is approximate, similar to the width of grain boundaries. Additionally, it should be understood that for TJs formed by grain boundaries of different types, e.g., low- and high-angle ones, the effective radius will differ. A change in radius should also be expected with temperature variation. This work is devoted to developing a method for determining the effective radius of a triple junction using the example of TJs of high-angle tilt grain boundaries with <100> and <111> misorientation axes in nickel. These axes were chosen as some of the most common in FCC crystals [19–22]. Only high-angle boundaries were considered, since low-angle ones represent an array of periodically arranged grain boundary dislocations [22–26], making it inappropriate to speak of a triple junction radius in this case. Nickel was selected as a well-studied typical FCC metal that also serves as the basis for many modern heat-resistant alloys.

The TJ radius can be determined from the spatial distribution of a specific characteristic, such as atomic potential energy, diffusion coefficient, free volume, etc., which distinguishes the defect against the background of the rest of the crystal. This work considers two methods: based on the self-diffusion intensity distribution [27] and based on the atomic potential energy distribution.

Description of the model

Interatomic interactions in the molecular dynamics model were described using a many-body potential developed in [28] based on the embedded atom method, accounting for the experimental properties of pure nickel: cohesive energy, lattice parameter, and elastic constants. In [28], it was shown that this potential successfully reproduces a wide range of other nickel properties, including energy characteristics of various defects, phonon spectrum, and thermal expansion. The potential used in this study and similar potentials have proven effective in various molecular dynamics simulations, including grain boundaries, plastic deformation, structural-phase transformations, self-diffusion, etc. [29–33].

The triple junction was created at the center of the computational cell by joining three grains misoriented relative to each other via rotation around an axis parallel to the triple junction line. The angles between the boundaries at the junction were initially set to 120° – as is known, most high-angle boundaries have approximately equal tension, so the angles between them at TJs are typically 120° [6,34,35]. The energy of low-angle and special boundaries is much lower than that of high-angle boundaries, their tension is lower, and the angles between such boundaries at TJs can significantly deviate from 120° [36]. This work considers triple junctions of only high-angle tilt boundaries with <100> and <111> misorientation axes. As noted in the Introduction, these axes are among the most common in FCC crystals [19–22]. Special grain-boundary misorientation angles were not considered because their atomic structures are exceptional, featuring a relatively high density of coincident lattice sites. As an example, arbitrary large angles ($\geqslant 15°$) were chosen. For the <100> axis the misorientation angles between grains were 18°, 18°, and 36°, and for the <111> axis they were 15°, 15°, and 30°.

After joining the three grains and removing excess atoms (those positioned too close to each other), a computational cell in the form of a cylinder was cut out. The triple junction was located along the central axis of the cylinder (Fig. 1). Periodic boundary conditions were applied along the cylinder axis, i.e., along the TJ line and tilt axes of the grains. Atoms on the lateral surface of the cylinder were fixed (highlighted in dark gray in Fig. 1). The cylinder diameter was approximately of 17.2 nm, length of 6.1 nm. The computational cell contained approximately 130 thousand atoms. When setting the temperature (during relaxation and diffusion simulation), thermal expansion was taken into account.

After the initial joining of the grains and cutting out the starting cylindrical computational cell, the stage of triple junction creation followed via melting and subsequent crystallization. The computational cell was heated to a temperature significantly exceeding the melting point of nickel (2500 K). After melting, isothermal holding was performed at a constant temperature of 1500 K using the Nose-Hoover thermostat for 500 ps. The fixed atoms on the lateral surface of the cylindrical computational cell simulated crystallization fronts from three different crystallization centers in this case. The crystallization front velocity is an order of magnitude lower than the speed of sound; defects and free volume during front motion are not "frozen" in place but form last – at the junction of crystalline phases with different orientations, i.e., in the grain boundary and triple junction regions (Fig. 2).

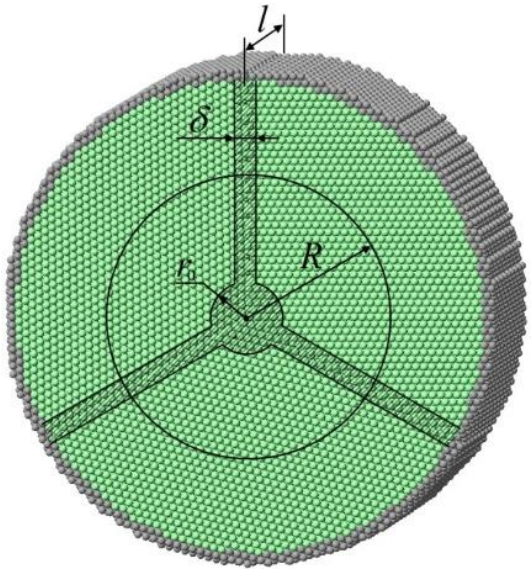


Fig. 1. Example of a cylindrical computational cell containing a <111> triple junction of tilt grain boundaries with misorientation angles of 15°, 15°, and 30°. Atoms colored dark gray remained immobile during the computer experiment. Hatched areas – grain boundaries and triple junction

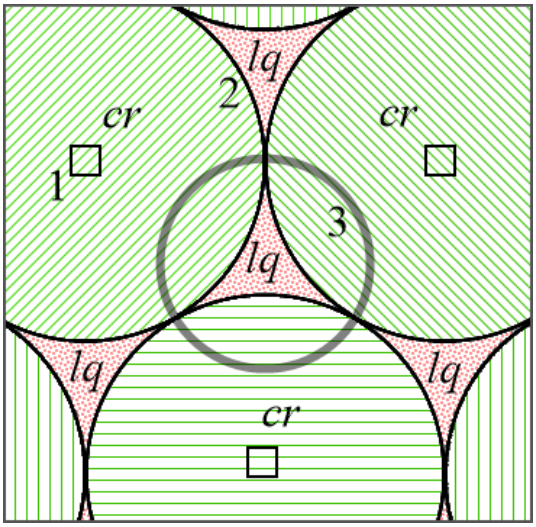


Fig. 2. Schematic illustration of excess free volume formation at a triple junction during the meeting of three crystallization fronts: *cr* – crystalline phase; *lq* – liquid phase; 1 – crystal nucleus; 2 – crystallization front; 3 – computational cell boundaries (Fig. 1)

In [18], we demonstrated that an important circumstance during the encounter of three crystallization fronts is that crystallization at triple junctions occurs last. Excess free volume concentrates precisely there. The density difference between the crystalline and liquid phases plays a crucial role: the density of the remaining liquid phase in the junction area, which has not yet crystallized, is typically much lower than that of the crystalline phase. This atomic deficiency for forming an "ideal" triple junction leads to the appearance of excess free volume, which, during crystallization, concentrates predominantly in the triple junction. In [18], a calculation was performed of the possible concentration of excess free volume in the junction formed during crystallization. It was found that the fraction of missing atoms (conditional vacancies) in the TJ area can reach 2 %.

In the present work, TJs with different contents of excess free volume – from 0 to 2 % conditional vacancies (removed atoms) – were considered. To introduce the free volume, atoms were removed at the initial simulation stage before melting the computational cell.

Diffusion radius of a triple junction

To determine the effective radius of the triple junction based on the self-diffusion intensity distribution, dependencies of the self-diffusion coefficient along the axis (*z*-axis) of the cylindrical computational cell (i.e., along the junction line) on the radius of the computational region *R* (Fig. 1) were obtained. The self-diffusion coefficient along the *z*-axis was calculated using the well-known formula:

$$D_z = \frac{\sum_{i=1}^{N}(z_{0i}-z_i)^2}{2Nt}. \quad (1)$$

Here z_{0i} and z_i are the initial and final coordinates of the i-th atom along the z-axis; N is the number of atoms in the computational region of radius R; t is the duration of the simulation.

The computational region for determining the self-diffusion coefficient had the shape of a cylinder with radius R and length l equal to that of the computational cell (Fig. 1). The center of this region did not always coincide with the cell center, since the junction could form off-center during crystallization. Therefore, prior to calculating the diffusion coefficient, a step was performed to select the center of the computational region such that it maximally coincided with the TJ center.

The idea of determining the triple junction radius using the $D_z(R)$ dependence is as follows. For a computational region radius R larger than the TJ radius r_0, the $D_z(R)$ dependence should be described by a simple formula, whereas within the junction area itself, i.e., for $R < r_0$ (Fig. 1), the character of the dependence should differ. The deviation between the approximation curve and the dependence obtained from the model gives the position of the effective TJ radius.

Figure 3 shows the dependencies of the self-diffusion coefficient D_z along the considered triple junctions on the computational region radius R at 1500 K. At other temperatures, the character of the dependencies was similar, with the main difference being in the diffusion coefficient values – it increased with rising temperature. As seen in Fig. 3, as the region radius R decreases, the self-diffusion coefficient increases. This provides clear evidence that the diffusive flux is concentrated along the triple junction.

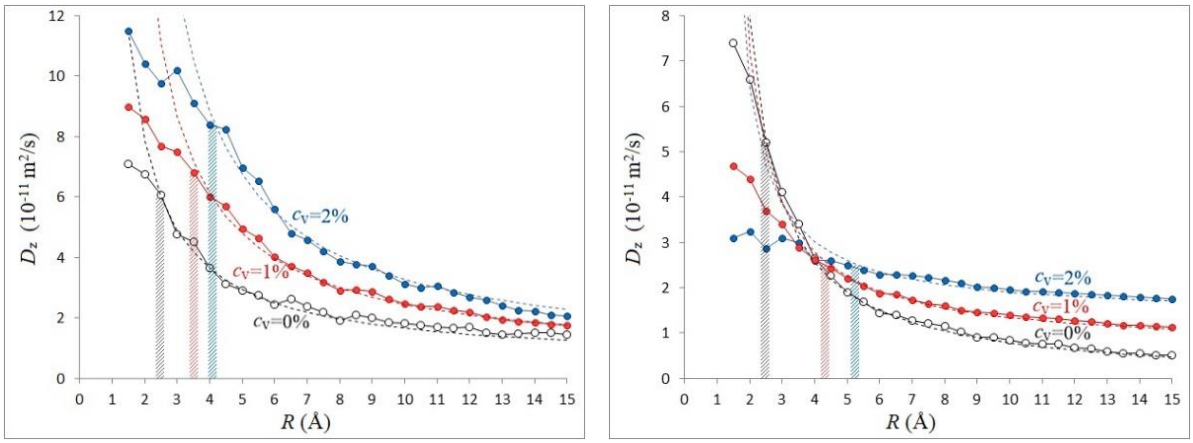


Fig. 3. Dependencies of the self-diffusion coefficient D_z along the triple junctions of <100> 18°/18°/36° (a) and <111> 15°/15°/30° tilt boundaries (b) on the computational region radius R at 1500 K. c_v – concentration of conditional vacancies. Dashed curves – approximations of the form $c_1/(R+c_2)+c_3$

With increasing excess free volume in the TJs, as seen from the presented graphs, diffusion proceeded more intensely – the self-diffusion coefficient increased with the number of introduced conditional vacancies.

Triple junctions and grain boundaries serve as channels of accelerated diffusion, along which diffusion proceeds much faster than in the pure crystal. In the ideal case, with zero channel width and identical diffusion intensity along all boundaries and the junction, the $D_z(R)$ dependence should have the form c/R, where c is a constant. However, due to differing diffusive permeabilities of the boundaries and errors in selecting the

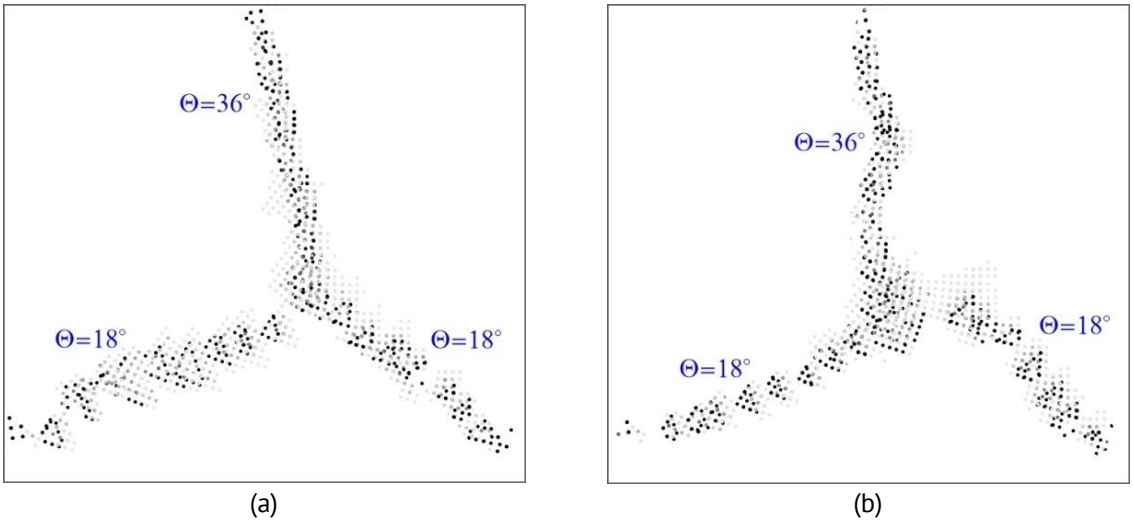
computational region center, the approximation curves were actually described by the equation $c_1/(R+c_2)+c_3$, where c_1, c_2, c_3 are constants (c_2 and c_3 were generally small and mainly served to refine the approximation). On Fig. 3, for each dependence obtained from the model, the corresponding approximation curves (shown as dashed lines) are provided. The effective radius of the triple junctions was determined from the deviation between the approximation curves and the model dependencies.

According to the obtained data, for the considered TJs into which no excess free volume was initially introduced – both of tilt boundaries with <100> and <111> disorientation axis – the effective diffusion radius was the same – 2.5 Å. Notably, the diameter of such a triple junction matches the experimental values for the width of high-angle grain boundaries in pure nickel – about 5 Å [37,38], which is typically determined from diffusion profiles. As noted in the Introduction, such junctions generally do not stand out from the grain boundaries that form them [15,16].

However, upon introducing additional free volume, the picture changes – the TJ diffusion radius increases, more strongly for the <111> boundary junction than for the <100> boundary one. With 2 % conditional vacancies introduced into the initial computational cell, the radius of the <111> 15°/15°/30° TJ more than doubles compared to the case without additional vacancies, reaching approximately 5.2 Å (Fig. 3(b)). The radius of the <100> 18°/18°/36° TJ with 2 % vacancies is smaller – about 4.1 Å. With temperature variation, the obtained diffusion radius values changed little, with fluctuations not exceeding 0.2 Å.

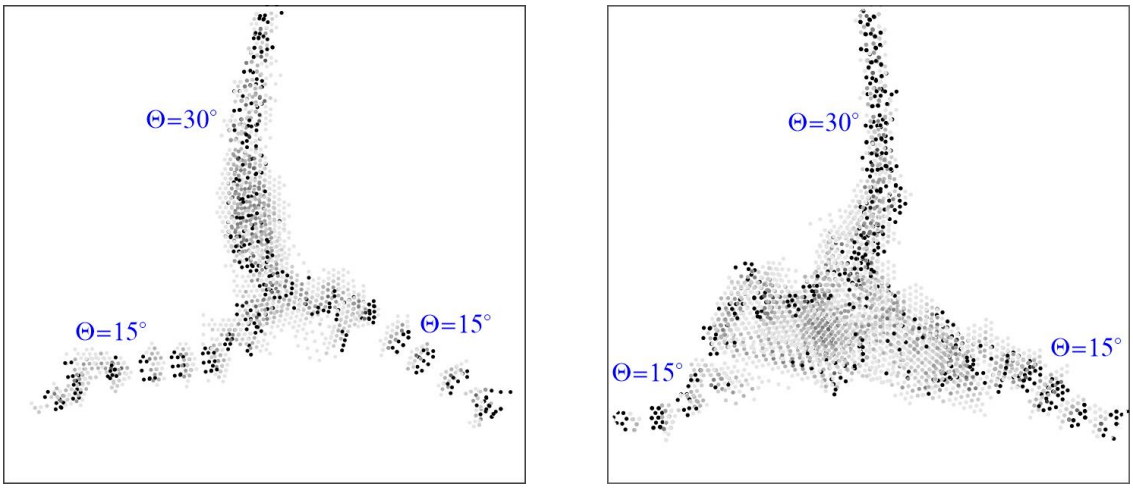
Energy radius of a triple junction

The effective radius based on the atomic potential energy distribution was determined by us using the same <100> 18°/18°/36° and <111> 15°/15°/30° TJs as examples. Figures 4 and 5 display the free volume distributions in the regions of the <100> (Fig. 4) and <111> (Fig. 5) TJs, obtained after crystallization and subsequent cooling with 1 % and 2 % vacancies introduced into the initial computational cell. The free volume was



(a) (b)

Fig. 4. Free volume distribution in the triple junction region of <100> tilt boundaries with misorientation angles of 18°, 18°, and 36°. Atoms are colored in various shades of gray depending on the free volume in their vicinity. From the initial computational cell were removed: (a) 1 % of atoms; (b) 2 % of atoms



(a) (b)

Fig. 5. Free volume distribution in the triple junction region of <111> tilt boundaries with misorientation angles of 15°, 15°, and 30°. Atoms are colored in various shades of gray depending on the free volume in their vicinity. From the initial computational cell were removed: (a) 1 % of atoms; (b) 2 % of atoms

visualized by calculating the average distance from each atom to its neighbors. If this average distance differed insignificantly from the distance corresponding to an ideal crystal, the atom was not depicted. Otherwise, the atom was colored in a particular shade of gray, depending on the average distance to its neighboring atoms.

As can be seen from Figs. 4 and 5, excess free volume concentrates predominantly in the grain boundary regions and, particularly, in the triple junction during the crystallization process. Moreover, the fraction of free volume increases as one approaches the junction area. This is better observed in the example of the <111> 15°/15°/30° TJ (Fig. 5) – by comparison, the <100> 18°/18°/36° TJ visually has a smaller radius associated with the free volume distribution, especially when 2 % conditional vacancies are introduced.

As can also be seen from Figs. 4 and 5, the triple junction does not have a regular shape – grain boundaries are typically slightly curved, and the junction area itself is neither perfectly circular nor defined by a sharp boundary. Therefore, the effective triple junction radius is a conditional concept, especially at a high excess free volume content (as, for example, in Fig. 5(b)).

To determine the effective TJ radius based on energy distribution, we used the quantity $\Delta E/(lR)$, where ΔE is the formation energy of the given structure in the computational cell, calculated as the difference between the potential energy of the computational cell and a perfect crystal containing the same number of atoms, l is the length of the cylindrical computational cell, and R is the radius of the computational region used to determine ΔE (Fig. 1). The center of the computational region was chosen to coincide as closely as possible with the TJ center.

In a general approximation, the quantity $\varepsilon(R)$ we considered consists of the sum of the energies of the boundaries and the triple junction itself:

$$\varepsilon(R) = \frac{\Delta E}{lR} \approx E_{b1} + E_{b2} + E_{b3} + \frac{E_{TJ}}{R}. \quad (2)$$

where E_{b1}, E_{b2}, and E_{b3} are the formation energies of the grain boundaries (eV/Å²); E_{TJ} is the formation energy of the triple junction (eV/Å). As $R \to \infty$, the quantity $\varepsilon(R)$ corresponds to the total surface tension of the three grain boundaries.

High-angle boundaries in most cases have similar formation energy values, which is why the majority of angles between them in TJs are approximately 120° [6,34,35]. If we assume that the formation energies of the boundaries, as well as the junction itself, are proportional to the volume of the defective region V (within the grain boundaries and the junction), then we can write $\Delta E \approx \alpha V$, where α is a proportionality coefficient. Letting δ be the width of the grain boundaries and r_0 be the radius of the triple junction, we can then write:

$$\varepsilon(R) = \frac{\Delta E}{lR} \approx \begin{cases} \alpha\pi R, & R \le r_0; \\ (\pi r_0 - 3\delta)\frac{\alpha r_0}{R} + 3\alpha\delta, & R > r_0. \end{cases} \quad (3)$$

Thus, according to the expression (3) we obtained, the dependence $\varepsilon(R)$ before $R \le r_0$ (that is, within the "region" of the triple junction) should be linear. Afterward, the character of the dependence changes: as R increases, the function $\varepsilon(R)$ asymptotically approaches a constant value – the total surface tension of the three grain boundaries.

The idea of determining the energy radius of a TJ is as follows. First, for the triple junctions obtained in the molecular dynamics model, the dependence of ε on R is constructed, where ε is calculated as the difference between the potential energies of the computational cell and a perfect crystal containing the same number of atoms. Then, the equations for the linear part of the obtained dependencies are determined, and the radius is found from the deviation of these lines from the main curves.

Figure 6 shows the $\varepsilon(R)$ dependencies obtained for the considered triple junctions upon introducing different numbers of vacancies into the initial computational cell. The dependencies were obtained after cooling the computational cells to 0 K to avoid the influence of thermal atomic vibrations. The dashed lines show the approximations of the linear parts.

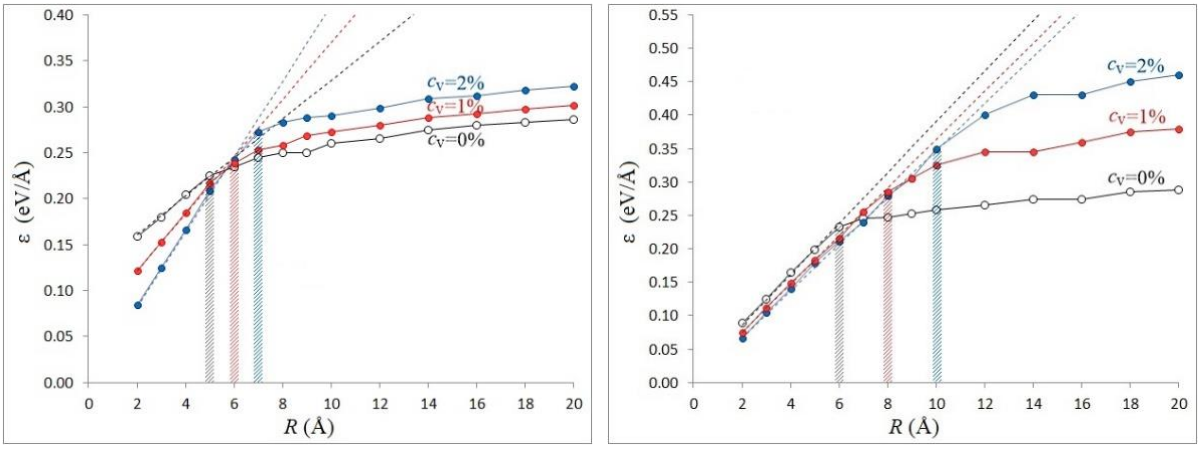


Fig. 6. Dependencies of the quantity ε on the computational region radius R for TJs: (a) <100> 18°/18°/36°; (b) <111> 15°/15°/30°. Dashed lines show the approximations of the linear parts of the dependencies

The $\varepsilon(R)$ dependencies obtained in the model have a form consistent with Eq. (3) – initially linear growth for $R \le r_0$, followed by an asymptotic approach to $3\alpha\delta$ for $R > r_0$. With an increase in the free volume introduced at the initial stage, the ε values are higher,

as expected. The greater the free volume, the more diffuse the triple junction boundaries are, resulting in a higher uncertainty for the derived radius. Comparing the TJs <100> (Fig. 6(a)) and <111> (Fig. 6(b)), it can be noted that in <100> boundary junctions, the free volume is concentrated more densely – this is evident not only from the comparatively smaller radius of the <100> TJs but also from the change in the slope of the initial linear part, from shallower at c_v=0 % to steeper at c_v=2 % (Fig. 6(a)). In the <111> TJs in our model, the free volume was dissipated less compactly, and the linear parts had the same slope (Fig. 6(b)).

Table 1 presents the effective radius values of the triple junctions under consideration for different free volume contents, obtained using both methods: the self-diffusion coefficient distribution and the atomic potential energy distribution.

Table 1. Effective diffusion and energy radii (Å) of the considered TJs as a function of the concentration of vacancies introduced into the initial computational cell

Method	**Triple junction**	**Concentration of vacancies c_v, %**		
		0	1	2
Diffusion	<100> 18°/18°/36°	2.5	3.5	4.1
	<111> 15°/15°/30°	2.5	4.3	5.2
Energy	<100> 18°/18°/36°	5	6	7
	<111> 15°/15°/30°	6	8	10

As noted above, the TJ radius is a conventional concept: the cross section of the defect itself may not be circular (for example, in Figs. 4 and 5), and its boundaries are blurred. In addition, the radius was determined visually at the point where the approximating curve diverges from the dependence obtained in the model. The points of the latter, as seen in Figs. 3 and 6, were also obtained with some errors. All these factors together produce an uncertainty in the determination of the TJ radius. When it was determined from the diffusion-intensity distribution, this uncertainty was about 0.2 Å in our model. When determined from the potential-energy distribution, it was approximately 0.5 Å. The difference in the errors of the two methods is apparently due to the fact that in the first case the radius being determined is not that of the defect itself but of the diffusion channel, which turns out to be narrower than the defective region. In addition, its boundaries are generally sharper compared with the pattern of energy distribution over atoms near the defect. In the second case, the defective region is more spatially smeared, especially when additional free volume is introduced, as in Figs. 4 and 5.

Both proposed methods for determining the TJ radius essentially describe different properties. When the radius is found from the diffusion-intensity distribution, what is actually determined is the radius of the diffusion channel associated with the triple junction. In the second case, when the radius is found from the distribution of atomic potential energy near the defect, the radius of the region that differs from the rest of the crystal is determined. This difference gradually decreases with distance from the defect center, and does so more smoothly than the diffusion intensity. Consequently, when determining the radius from the energy distribution it is harder to pinpoint the divergence between the theoretical and modelled curves (Fig. 6), which accounts for the comparatively larger error of this method. Thus, it would be incorrect to directly compare the accuracy of the two methods and claim that one is more precise while the other is

cruder – as noted above, the methods describe different properties of the TJ, and both are useful for different tasks. The diffusion-based method is obviously appropriate when considering diffusion and defect migration, while the energy-based method is appropriate for studying interactions between TJs and other defects.

Conclusions

In the present work, two methods for determining the effective radius of grain boundary triple junctions are proposed, based on the analysis of the self-diffusion coefficient distribution and the atomic potential energy distribution in the junction region. Both methods were examined using high-angle tilt boundary triple junctions with <100> and <111> disorientation axes, containing varying amounts of excess free volume. The triple junctions were generated in the model by simulating melt crystallization from three differently oriented crystalline nuclei. Excess free volume was introduced into the triple junction by removing the corresponding number of atoms from the initial computational cell. During crystallization, the introduced free volume concentrated predominantly in the grain boundary and triple junction regions, with the free volume fraction increasing as one approached the junction point.

With an increase in excess free volume in the TJs, self-diffusion proceeded more intensely. Furthermore, the diffusion intensity within the triple junction itself was generally non-uniformly distributed and increased toward the junction center.

It was shown that the effective TJ radius, determined by both methods – based on the diffusion coefficient distribution and the atomic energy distribution – increases with the free volume content. In the considered <100> tilt boundary junctions, the free volume concentrated more densely during crystallization, resulting in a smaller radius compared to the <111> tilt boundary junctions. In the former case, using the diffusion method, the junction radius increased from 2.5 Å without additional vacancies in the initial computational cell to 4.1 Å when 2 % vacancies were introduced prior to crystallization. For the <111> boundary junction, the diffusion radius increased from 2.5 to 5.2 Å. The method based on the analysis of atomic potential energy distribution yielded significantly larger values for the effective triple junction radius: for <100> junctions – from 5 Å without vacancies to 7 Å with 2 % vacancies; for <111> junctions – from 6 to 10 Å. Based on the results obtained for the TJs studied in nickel, one can predict the radii of analogous junctions in other FCC metals by, for example, scaling with the ratio of their lattice parameters.

CRediT authorship contribution statement

Gennady M. Poletaev: conceptualization, writing – review & editing; **Yuriy V. Bebikhov**: investigation, data curation; **Alexander S. Semenov**: investigation, data curation; **Roman Y. Rakitin**: investigation; **Darya V. Novoselova**: investigation.

Conflict of interest

The authors declare that they have no conflict of interest.

References

1. Palumbo G, Aust KT. A coincident axial direction (CAD) approach to the structure of triple junctions in polycrystalline materials. *Scripta Metallurgica et Materialia*. 1990;24: 1771–1776.
2. Wegner M, Leuthold J, Peterlechner M, Song X, Divinski SV, Wilde G. Grain boundary and triple junction diffusion in nanocrystalline copper. *Journal of Applied Physics*. 2014;116: 093514.
3. Gutkin MY, Ovidko IA. Yield stress of nanocrystalline materials. In: *Plastic Deformation in Nanocrystalline Materials. Springer Series in Materials Science, vol 74*. Berlin: Springer; 2004. p.7–48.
4. Rodriguez P, Sundararaman D, Divakar R, Raghunathan VS. Structure of grain boundaries in nanocrystalline and quasicrystalline materials. *Chemistry for Sustainable Development*. 2000;8: 69–72.
5. Kang J, Walter K, Bale H, Shahani AJ. Percolation of grain boundaries and triple junctions in three-dimensions: A test of theory. *Acta Materialia*. 2022;240: 118316.
6. Patrick MJ, Rohrer GS, Chirayutthanasak O, Ratanaphan S, Homer ER, Hart GLW, Epshteyn Y, Barmak K. Relative grain boundary energies from triple junction geometry: Limitations to assuming the Herring condition in nanocrystalline thin films. *Acta Materialia*. 2023;242: 118476.
7. Tuchinda N, Schuh CA. Triple junction solute segregation in Al-based polycrystals. *Physical Review Materials*. 2023;7: 023601.
8. Zhu S, Borodin E, Jivkov AP. Triple junctions network as the key pattern for characterisation of grain structure evolution in metals. *Materials and Design*. 2021;198: 109352.
9. Qian Y, Silva A, Yu E, Anderson CL, Liu Y, Theis W, Ercius P, Xu T. Crystallization of nanoparticles induced by precipitation of trace polymeric additives. *Nature Communications*. 2021;12: 2767.
10. Yadav B, Muralikrishna GM, Vaidya M, Wilde G, Divinski SV. Grain boundary diffusion in compositionally complex alloys: A comprehensive review. *International Materials Reviews*. 2026;71(2): 129–177.
11. Schweizer P, Sharma A, Petho L, Huszar E, Vogl LM, Michler J, Maeder X. Atomic scale volume and grain boundary diffusion elucidated by in situ STEM. *Nature Communications*. 2023;14: 7601.
12. Rad MT, Boussinot G, Apel M. Geometry of triple junctions during grain boundary premelting. *Physical Review Letters*. 2021;127: 225701.
13. Newton, Basak A. Multiphase-field approach to grain boundary- and triple junction-induced barrierless premelting of polycrystals and size-effect. *The Journal of Chemical Physics*. 2025;162: 124714.
14. Poletaev G, Rakitin R, Bebikhov Y, Semenov A. Molecular dynamics study of melting initiation at tilt grain boundaries depending on their misorientation angle in aluminum. *Physica Scripta*. 2025;100: 015988.
15. Frolov T, Mishin Y. Molecular dynamics modeling of self-diffusion along a triple junction. *Physical Review B*. 2009;79: 174110.
16. Adlakha I, Solanki KN. Structural stability and energetics of grain boundary triple junctions in face centered cubic materials. *Scientific Reports*. 2015;5: 8692.
17. Kozlov EV, Koneva NA, Popova NA. Grain structure, geometrically necessary dislocations and second-phase particles in polycrystals of micro- and mesolevels. *Physical Mesomechanics*. 2009;12: 280–292.
18. Poletaev GM, Novoselova DV, Kaygorodova VM. The causes of formation of the triple junctions of grain boundaries containing excess free volume in fcc metals at crystallization. *Solid State Phenomena*. 2016;247: 3–8.
19. Pan Y, Adams BL. On the CSL grain boundary distributions in polycrystals. *Scripta Metallurgica*. 1994;30(8): 1055–1060.
20. Kurzydlowski KJ, Ralph B, Bucki JJ, Garbacz A. The grain boundary character distribution effect on the flow stress of polycrystals: The influence of crystal lattice texture. *Materials Science and Engineering A*. 1996;205: 127–132.
21. Rohrer GS. The distribution of grain boundary planes in polycrystals. *Journal of the Minerals, Metals & Materials Society*. 2007;59: 38–42.
22. Zhu Q, Huang Q, Guang C, An X, Mao SX, Yang W, Zhang Z, Gao H, Zhou H, Wang J. Metallic nanocrystals with low angle grain boundary for controllable plastic reversibility. *Nature Communications*. 2020;11: 3100.
23. Tschopp MA, Mcdowell DL. Asymmetric tilt grain boundary structure and energy in copper and aluminium. *Philosophical Magazine*. 2007;87(25): 3871–3892.
24. Gutkin MY, Rzhavtsev EA. Dynamics of formation of low-angle tilt boundaries in metals and alloys at high loading rates. *Physics of the Solid State*. 2015;57: 2447–2457.
25. Zhou G, Huang Q, Chen Y, Yu X, Zhou H. Annihilation mechanism of low-angle grain boundary in nanocrystalline metals. *Metals*. 2022;12: 451.

26. Guo H, Zhao Y, Sun Y, Tian J, Hou H, Qi K, Tian X. Phase field crystal study of grain boundary structure and annihilation mechanism in low-angle grain boundary. *Superlattices and Microstructures*. 2019;129: 163–175.
27. Poletaev GM, Novoselova DV, Zorya IV, Starostenkov MD. Diffusion radius of triple junctions of tilt boundaries in Ni. *Materials Physics and Mechanics*. 2017;30(1): 68–74.
28. Purja Pun GP, Mishin Y. Development of an interatomic potential for the Ni-Al system. *Philosophical Magazine*. 2009;89: 3245–3267.
29. Levchenko EV, Ahmed T, Evteev AV. Composition dependence of diffusion and thermotransport in Ni-Al melts: a step towards molecular dynamics assisted databases. *Acta Materialia*. 2017;136: 74–89.
30. Poletaev G, Sannikov A, Gafner Y, Gafner S, Zorya I. Mechanical properties of crystalline and amorphous nickel nanoparticles: molecular dynamics simulation. *Journal of Nanoparticle Research*. 2025;27: 153.
31. Poletaev GM, Bebikhov YV, Semenov AS, Starostenkov MD. Self-diffusion in melts of Ni-Al and Ti-Al systems: molecular dynamics study. *Letters on Materials*. 2021;11(4): 438–441.
32. Pei Q-X, Jhon MH, Quek SS, Wu Z. A systematic study of interatomic potentials for mechanical behaviours of Ti-Al alloys. *Computational Materials Science*. 2021;188: 110239.
33. Poletaev GM, Bebikhov YV, Semenov AS, Sitnikov AA, Yakovlev VI. Molecular dynamics study of the dissolution of titanium nanoparticles in aluminum. *Materials Physics and Mechanics*. 2023;51(5): 9–15.
34. Fortes MA, Deus AM. Effects of triple grain junctions on equilibrium boundary angles and grain growth kinetics. *Materials Science Forum*. 2004;455–456: 648–652.
35. Yang CC, Rollett AD, Mullins WW. Measuring relative grain boundary energies and mobilities in an aluminum foil from triple junction geometry. *Scripta Materialia*. 2001;44: 2735–2740.
36. Perevalova OB, Konovalova EV, Koneva NA, Kozlov EV. Energy of grain boundaries of different types in fcc solid solutions, ordered alloys and intermetallics with L12 superstructure. *Journal of Materials Science and Technology*. 2003;19(6): 593–596.
37. Divinski SV, Reglitz G, Wilde G. Grain boundary self-diffusion in polycrystalline nickel of different purity levels. *Acta Materialia*. 2010;58: 386–395.
38. Bokstein B, Rodin A. Grain boundary diffusion and grain boundary segregation in metals and alloys. *Diffusion Foundations*. 2014;1: 99–122.